

A Bio-Inspired Multi-Exposure Fusion Framework for Low-light Image Enhancement

Zhenqiang Ying, *Student Member, IEEE*, Ge Li, *Member, IEEE*, and Wen Gao, *Fellow, IEEE*

Abstract—Low-light images are not conducive to human observation and computer vision algorithms due to their low visibility. Although many image enhancement techniques have been proposed to solve this problem, existing methods inevitably introduce contrast under- and over-enhancement. Inspired by human visual system, we design a multi-exposure fusion framework for low-light image enhancement. Based on the framework, we propose a dual-exposure fusion algorithm to provide an accurate contrast and lightness enhancement. Specifically, we first design the weight matrix for image fusion using illumination estimation techniques. Then we introduce our camera response model to synthesize multi-exposure images. Next, we find the best exposure ratio so that the synthetic image is well-exposed in the regions where the original image is under-exposed. Finally, the enhanced result is obtained by fusing the input image and the synthetic image according to the weight matrix. Experiments show that our method can obtain results with less contrast and lightness distortion compared to that of several state-of-the-art methods.

Index Terms—Image enhancement, contrast enhancement, exposure compensation, exposure fusion.

I. INTRODUCTION

WITH the development of photographic techniques, the image quality is greatly improved in both resolution and bit-depth. However, images captured by standard imaging devices often suffer from low visibility in non-uniform illuminated environments such as back lighting, nighttime and low-light indoor scene. Those images may lose information in under-exposed regions, making the image content invisible to human eyes. Since the camera dynamic range is limited, if we increase camera exposure to reveal the information of under-exposed regions, the well-exposed regions will be over-exposed or even saturated. To address the problem, many image enhancement techniques have been proposed including histogram-based methods [1], [2], [3], [4], [5], [6], [7], [8], [9], [10], [11], [12], [13], Retinex-based methods [14], [15], [16], [17], [18], [19], [20], Logarithmic Image Processing methods [21], [22], and filtering-based methods [23], [24], [25], [26], [27]. Although some methods can obtain results with good subjective quality, those results may not accurately

This work was supported by the grant of National Science Foundation of China (No.U1611461), Shenzhen Peacock Plan (20130408-183003656), and Science and Technology Planning Project of Guangdong Province, China (No. 2014B090910001). This paper was recommended by Associate Editor X. XX.

Z. Ying, G. Li, and W. Gao are with the School of Electronic and Computer Engineering, Shenzhen Graduate School, Peking University, 518055 Shenzhen, China (e-mail: zqying@pku.edu.cn; geli@ece.pku.edu.cn; wgao@pku.edu.cn).

Color versions of one or more of the figures in this paper are available online at <http://ieeexplore.ieee.org>.

Digital Object Identifier XX.XXXX/TCYB.20XX.XXXXXXX

Manuscript received XXX XX, 20XX; revised XXX XX, 20XX.

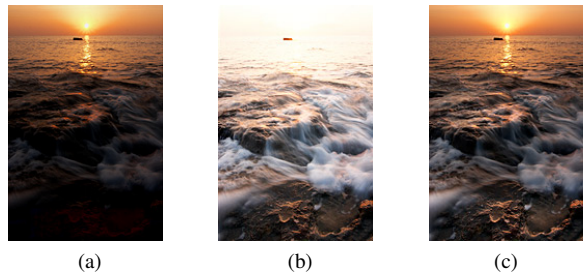


Fig. 1. Our mental image is a fused version of different eye exposure. (dynamically adjusting). (a) Eye focuses on background. (b) Eye focuses on foreground. (c) Our mental image. [28]

reflect the true lightness and contrast of the scene. So, accurate light and contrast enhancement based on a single image is still a challenging problem.

With a set of different exposure images in the same scene, High Dynamic Range (HDR) techniques can synthesize images that are close to the perceived scene. We know that the camera and the human eye have a lot of similarities, then, why we can perceive an image that is well-exposed everywhere while the camera cannot? The reason lies in the post-processing in our brains that have an image fusion mechanism similar to HDR technique [28]. Human eye exposure changes with its focus point, resulting in multi-exposure image set which is then sent to the brain. Although each one of those images suffers from under-exposed or over-exposed problem in some regions, our brain can fuse these images into an image that is free from under- and over-exposed problems, as shown in Fig. 1.

Can we introduce this fusion mechanism of human visual system (HVS) to help build an accurate image enhancement algorithm? Although many exposure fusion techniques have been proposed in the domain of HDR, the additional images taken with different exposures are often not available for the low-light enhancement problem. Fortunately, those images are highly correlated. The mapping function between two images that only differ in exposure is called Brightness Transform Function (BTF). Therefore, we can first use BTF to generate a series of multi-exposure images and then fuse those images to obtain the enhanced result.

In this paper, we propose a multi-exposure fusion framework inspired by the HVS. There are two stages in our framework: Eye Exposure Adjustment and Eye Exposure Adjustment. The first stage simulates the human eye to adjust the exposure, generating an multi-exposure image set. The second stage simulates the human brain to fuse the generated

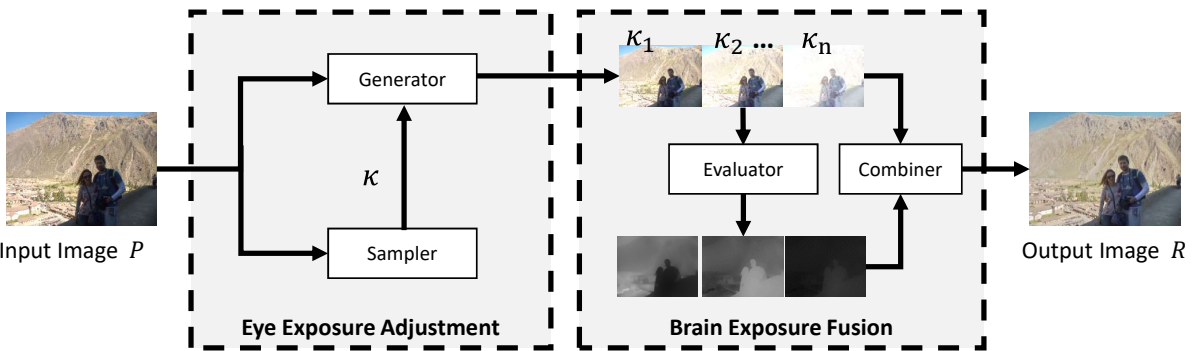


Fig. 2. Our framework.

images into the final enhanced result. Based on our framework, we propose a dual-exposure fusion method. Specifically, we first employ the illumination estimation techniques to build the weight matrix for image fusion. Then we derive our camera response model based on observation. Next, we find the optimal exposure for our camera response model to generate the synthetic image that is well-exposed in the regions where the original image is under-exposed. Finally, we obtain the enhanced results by fusing the input image with the synthetic image using the weight matrix. Experiments on five challenging datasets are conducted to reveal the advantages of our method in comparison with other state-of-the-art methods.

II. RELATED WORK

In general, image enhancement techniques can improve the subjective visual quality of input images and support the extraction of valuable information for some computer vision techniques [29], [16]. Low-light image enhancement, as one of enhancement techniques, can reveal the information of the under-exposed regions in an image. Broadly speaking, existing low-light image enhancement techniques can be divided into two major categories: global enhancement and local enhancement.

A. Global Enhancement Algorithms

Global enhancement performs same processing on all image pixels regardless of their spatial distribution. Linear amplifying is a simple and straightforward global enhancement method. However, bright regions might be saturated after linear amplifying, causing some detail loss to the enhanced results. To avoid the problem, some image enhancement methods adopt non-linear monotonic functions (e.g. power-law [30], logarithm [31] and gamma function [32]) to perform enhancements. As another way to avoid saturation, histogram equalization (HE) [33] can improve the contrast effectively and became a widely-used technique. Many extensions of HE are proposed to take some restrictions into account such as brightness preservation [29], [34], [10] and contrast limitation [35]. By extending the notion of the histogram, some algorithms take spatial image features into consideration to further improve the performance [3], [6], [7]. However, global enhancement may suffer from detail loss in some local areas

because a global processing can not ensure all local areas be well enhanced.

B. Local Enhancement Algorithms

By making use of spatial information directly, local enhancement can achieve better results and become the mainstream of recent techniques. Local histogram equalization [36], [37] adopts the sliding window strategy to perform HE locally. Based on the observation that the inverted low-light images are closer to hazy images, dehazing techniques are borrowed to solve low-light image enhancement in some methods [38], [39]. However, the basic models of above methods are lacking in physical explanation [14]. To provide a physical meaningful model for image enhancement, Retinex theory assumes that the amount of light reaching observers can be decomposed into two parts: illumination and scene reflection. Most Retinex-based methods get enhanced results by removing the illumination part [18], [20], [15] while others [40], [16], [14] keep a portion of the illumination to preserve naturalness. Fu *et al.* [41] adjust the illumination components by fusing it with two enhanced illumination. As far as we know, there is no multi-exposure fusion method for this task since lowlight enhancement problem usually takes a single image as input.

III. MULTI-EXPOSURE FUSION FRAMEWORK

Our framework mainly consists of four main components: the first component, named Multi-Exposure Sampler, determines how many images are required and the exposure ratio of each image to be fused; the second component, named Multi-Exposure Generator, use a camera response model and the specified exposure ratio to synthetic multi-exposure images; the third component, named Multi-Exposure Evaluator, determines the weight map of each image when fusing; the last component, named Multi-Exposure Combiner, is to fuse the generated images to the final enhanced result based on the weight maps. In this section, we introduce them one by one.

A. Multi-Exposure Sampler

Before we generate multi-exposure images, we need to determine how many images are required and their exposure ratios. Since some images in the multi-exposure set cannot

provide additional information, taking these images into consideration is a waste of computation resources and may even deteriorate the fused result. A good sampler can use as few images as possible to reveal all the information in a scene by choosing appropriate exposure ratios. The output of the sampler is a set of exposure ratios $\{k_1, k_2, \dots, k_N\}$ where N is the number of the images to be generated.

B. Multi-Exposure Generator

As aforementioned, images taken with different exposures are correlated. Multi-Exposure Generator maps the input image into multi-exposure images according to the specified exposure ratio set. The key part of the Multi-Exposure Generator is the camera response model used to find an appropriate BTF for mapping. Given an exposure ratio k_i and a BTF g , we can map the input image \mathbf{P} to the i -th image in the exposure set as

$$\mathbf{P}_i = g(\mathbf{P}, k_i). \quad (1)$$

C. Multi-Exposure Evaluator

To estimate the wellness of each pixel in the generated images. The Multi-Exposure Evaluator takes in an image and outputs a weight matrix that indicates the wellness of each pixel. The weight matrix is nonuniform for all pixels: the well-exposed pixels are given a big weight while the poor-exposed pixels are given a small weight. After all images are evaluated, the output matrices are pixel-wise normalized to ensure their summation equals one for each pixel as

$$\widetilde{\mathbf{W}}_i = \mathbf{W}_i \oslash \sum_{i=1}^N \mathbf{W}_i, \quad (2)$$

where \oslash is the element-wise division, and \mathbf{W}_i and $\widetilde{\mathbf{W}}_i$ are the i -th matrix before and after normalization, respectively.

D. Multi-Exposure Combiner

To obtain an image with all pixel well-exposed, we can simply fuse these images based on the weight matrix as

$$\mathbf{R}^c = \sum_{i=1}^N \widetilde{\mathbf{W}}_i \circ \mathbf{P}_i^c, \quad (3)$$

where c is the index of three color channels and \mathbf{R} is the enhanced result. Other fusion techniques like multi-scale fusion [42] and Boosting Laplacian Pyramid fusion [43] can also be used to obtain a better fusion results.

IV. DUAL-EXPOSURE FUSION ALGORITHM

In this section, we use the proposed framework to design a low-light image enhancement algorithm. To reduce complexity, we only generate one image with appropriate exposure and obtain the enhanced result by fusing the input image and the generated one. Based on our framework, the fused image is defined as

$$\mathbf{R}^c = \hat{\mathbf{W}} \circ \mathbf{P}^c + (1 - \hat{\mathbf{W}}) \circ g(\mathbf{P}^c, \hat{k}). \quad (4)$$

The enhancement problem can be divided into three parts: the determination of multi-exposure Evaluator ($\hat{\mathbf{W}}$), multi-exposure generator (g), and multi-exposure sampler (\hat{k}). In the following subsections, we solve them one by one.

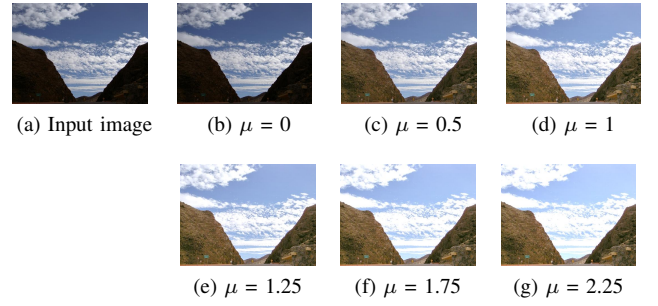


Fig. 3. The enhanced results using different μ .

A. Dual-Exposure Evaluator

The design of \mathbf{W} is key to obtaining an enhancement algorithm that can enhance the low contrast of under-exposed regions while the contrast in well-exposed regions preserved. We need to assign big weight values to well-exposed pixels and small weight values to under-exposed pixels. Intuitively, the weight matrix is positively correlated with the scene illumination. Since highly illuminated regions have big possibility of being well-exposed, they should be assigned with big weight values to preserve their contrast. We calculate the weight matrix as

$$\hat{\mathbf{W}} = \mathbf{T}^\mu \quad (5)$$

where \mathbf{T} is the scene illumination map and μ is a parameter controlling the enhancement degree. When $\mu = 0$, the resulting \mathbf{R} is equal to \mathbf{P} , i.e., no enhancement is performed. When $\mu = 1$, both the under-exposed pixels and well-exposed pixels are enhanced. When $\mu > 1$, pixels may get saturated and the resulting \mathbf{R} suffers from detail loss. As shown in Fig. 3. In order to perform enhancement while preserving the well-exposed regions, we set μ to 0.5. The scene illumination map \mathbf{T} is estimated by solving an optimization problem.

1) *Optimization Problem:* The lightness component can be used as an estimation of scene illumination. We adopt the lightness component as the initial estimation of illumination:

$$\mathbf{L}(x) = \max_{c \in \{R, G, B\}} \mathbf{P}_c(x) \quad (6)$$

for each individual pixel x . Ideal illumination should have local consistency for the regions with similar structures. In other words, \mathbf{T} should keep the meaningful structures of the image and remove the textural edges. As in [14], we refine \mathbf{T} by solving the following optimization equation:

$$\min_{\mathbf{T}} \|\mathbf{T} - \mathbf{L}\|_2^2 + \lambda \|\mathbf{M} \circ \nabla \mathbf{T}\|_1, \quad (7)$$

where $\|\cdot\|_2$ and $\|\cdot\|_1$ are the ℓ_2 and ℓ_1 norm, respectively. The first order derivative filter ∇ contains $\nabla_h \mathbf{T}$ (horizontal) and $\nabla_v \mathbf{T}$ (vertical). \mathbf{M} is the weight matrix and λ is the coefficient. The first term of this equation is to minimize the difference between the initial map \mathbf{L} and the refined map \mathbf{T} , while the second term maintains the smoothness of \mathbf{T} .

The design of \mathbf{M} is important for the illumination map refinement. A major edge in a local window contributes more similar-direction gradients than textures with complex patterns [44]. Therefore, the weight in a window that contains

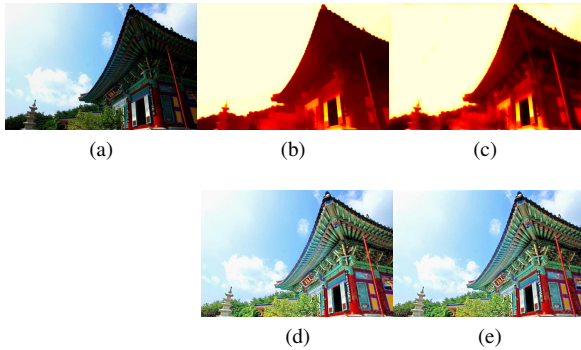


Fig. 4. (a) Input image. (b) Estimated illumination map by [14] (0.21s). (c) Our illumination map (0.15s). (d) Enhanced result using (b). (e) Enhanced result using (c).

meaningful edges should be smaller than that in a window only containing textures. As a result, we design the weight matrix as

$$\mathbf{M}_d(x) = \frac{1}{|\sum_{y \in \omega(x)} \nabla_d \mathbf{L}(y)| + \epsilon}, \quad d \in \{h, v\}, \quad (8)$$

where $|*|$ is the absolute value operator, $\omega(x)$ is the local window centered at the pixel x and ϵ is a very small constant to avoid the zero denominator.

2) *Closed-Form Solution*: To reduce the complexity, we approximate Eq. 7 as in [14]:

$$\min_{\mathbf{T}} \sum_x \left((\mathbf{T}(x) - \mathbf{L}(x))^2 + \lambda \sum_{d \in \{h, v\}} \frac{\mathbf{M}_d(x) (\nabla_d \mathbf{T}(x))^2}{|\nabla_d \mathbf{L}(x)| + \epsilon} \right). \quad (9)$$

As can be seen, the problem now only involves quadratic terms. Let \mathbf{m}_d , \mathbf{l} , \mathbf{t} and $\nabla_d \mathbf{l}$ denote the vectorized version of \mathbf{M}_d , \mathbf{L} , \mathbf{T} and $\nabla_d \mathbf{L}$ respectively. Then the solution can be directly obtained by solving the following linear function.

$$(\mathbf{I} + \lambda \sum_{d \in \{h, v\}} (\mathbf{D}_d^\top \text{Diag}(\mathbf{m}_d \oslash (|\nabla_d \mathbf{l}| + \epsilon)) \mathbf{D}_d) \mathbf{l} = \mathbf{1} \quad (10)$$

where \oslash is the element-wise division, \mathbf{I} is the unit matrix, the operator $\text{Diag}(\mathbf{v})$ is to construct a diagonal matrix using vector \mathbf{v} , and \mathbf{D}_d are the Toeplitz matrices from the discrete gradient operators with forward difference.

The main difference between our illumination map estimation method and that in [14] is the design of weight matrix \mathbf{M} . We adopt a simplified strategy which can yield similar results as in [14]. As shown in Fig. 4, although the illumination map in [14] is sharper than ours, our method is more time-saving while the two enhanced results show no significant visual difference.

B. Dual-Exposure Generator

In this section, we present a camera response model to implement the Multi-Exposure Generator. A camera response model consists of two parts: Camera Response Function (CRF) model and BTF model. The parameters of CRF model is determined only by camera while that of BTF model is determined by camera and exposure ratio. In this subsection, we

first propose our BTF model based on the observation of two different exposure images. Then we derive the corresponding CRF model by solving the comparametric equation. Finally, we discuss how to determine the model parameters and present the final form of g .

1) *BTF Estimation*: To estimate the BTF g , we select a pair of images \mathbf{P}_0 and \mathbf{P}_1 that differ only in exposure. Then we plot their histograms of each color channel, as shown in Fig. 5. Noticing that the histograms of the under-exposed image mainly concentrate in low-brightness area, if we perform linear amplification of pixel values before traditional gamma correction, then the resulting image will be very close to the real well-exposed image. Therefore, we can use a two-parameter function to describe the BTF model as

$$\mathbf{P}_1 = g(\mathbf{P}_0, k) = \beta \mathbf{P}_0^\gamma, \quad (11)$$

where β and γ are parameters in our BTF model related to exposure ratio k . The observation also shows that different color channels have approximately same model parameters. The underlying reason is that the response curves of different color channels are approximately identical for general cameras.

2) *CRF Estimation*: In our BTF model, β and γ are determined by the camera parameters and exposure ratio k . To find their relationship, we need to obtain the corresponding CRF model. The CRF model can be derived by solving the following comparametric equation (plug $g = \beta f^\gamma$ to $f(kE) = g(f(E))$):

$$f(kE) = \beta f(E)^\gamma. \quad (12)$$

The closed-form solution of f is provided in as follows (see Appendix for detail):

$$f(E) = \begin{cases} e^{b(1-E^a)}, & \text{if } \gamma \neq 1, \\ E^c, & \text{if } \gamma = 1. \end{cases} \quad (13)$$

where a and b are model parameters in the case of $\gamma \neq 1$:

$$a = \log_k \gamma, \quad b = \frac{\ln \beta}{1 - \gamma}; \quad (14)$$

And c is a model parameter in the case of $\gamma = 1$:

$$c = \log_k \beta. \quad (15)$$

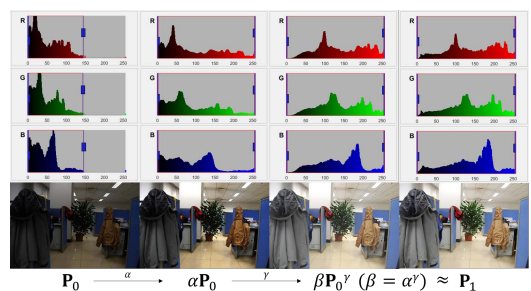


Fig. 5. Observation. From left to right: An under-exposure image \mathbf{P}_0 , apply multiplication $\alpha \mathbf{P}_0$, apply gamma function $(\alpha \mathbf{P}_0)^\gamma$ and the well-exposure image \mathbf{P}_1 under the same scene. The histograms of red, green and blue color channels are plotted above the corresponding image respectively.



Fig. 6. Examples of multi-exposure image sets and their entropy values. The red bar on the left of each image shows the exponential of its entropy value.

Two CRF models can be derived from two cases of Eq. 13. When $\gamma = 1$, the CRF model is a power function and the BTF model is a simple linear function. As some camera manufacturers design f to be a gamma curve, it can fit these cameras perfectly. When $\gamma \neq 1$, the CRF model is a two-parameter function and the BTF model is a non-linear function. Since the BTF is non-linear for most cameras, we mainly consider the case of $\gamma \neq 1$. Our BTF g is solved as

$$g(\mathbf{P}, k) = e^{b(1-k^a)} \mathbf{P}^{(k^a)}. \quad (16)$$

where β and γ are two model parameters that can be calculated from camera parameters a, b and exposure ratio k . We assume that no information about the camera is provided and use a fixed camera parameters ($a = -0.3293, b = 1.1258$) that can fit most cameras.

C. Dual-Exposure Sampler

As aforementioned, our algorithm only generate one image. So, in this subsection, we only need to determinate the optimal exposure ratio of the generated image. In order to represent as many information as possible using only the input image and the generated one, we find the best exposure ratio so that the synthesis image is well-exposed in the regions where the original image under-exposed.

First, we exclude the well-exposed pixels and obtain an image that is globally under-exposed. We simply extract the low illuminated pixels as

$$\mathbf{Q} = \{\mathbf{P}(x) | \mathbf{T}(x) < 0.5\}, \quad (17)$$

where \mathbf{Q} contains only the under-exposed pixels.

The brightness of the images under different exposures changes significantly while the color is basically the same. Therefore, we only consider the brightness component when estimating k . The brightness component \mathbf{B} is defined as the geometric mean of three channel:

$$\mathbf{B} := \sqrt[3]{\mathbf{Q}_r \circ \mathbf{Q}_g \circ \mathbf{Q}_b}, \quad (18)$$

where $\mathbf{Q}_r, \mathbf{Q}_g$ and \mathbf{Q}_b are the red, green and blue channel of the input image \mathbf{Q} respectively. We use the geometric mean instead of other definitions (e.g. arithmetic mean and weighted

arithmetic mean) since it has the same BTF model parameters (β and γ) with all three color channels, as shown in Eq. 19.

$$\begin{aligned} \mathbf{B}' &:= \sqrt[3]{\mathbf{Q}'_r \circ \mathbf{Q}'_g \circ \mathbf{Q}'_b} \\ &= \sqrt[3]{(\beta \mathbf{Q}_r^\gamma) \circ (\beta \mathbf{Q}_g^\gamma) \circ (\beta \mathbf{Q}_b^\gamma)} = \beta (\sqrt[3]{\mathbf{Q}_r \circ \mathbf{Q}_g \circ \mathbf{Q}_b})^\gamma \\ &= \beta \mathbf{B}^\gamma. \end{aligned} \quad (19)$$

The visibility of a well-exposed image is higher than that of an under/over-exposed image and it can provide a richer information for human. Thus, the optimal k should provide the largest amount of information. To measure the amount of information, we employ the image entropy which is defined as

$$\mathcal{H}(\mathbf{B}) = - \sum_{i=1}^N p_i \cdot \log_2 p_i, \quad (20)$$

where p_i is the i -th bin of the histogram of \mathbf{B} which counts the number of data valued in $[\frac{i}{N}, \frac{i+1}{N})$ and N is the number of bins (N is often set to be 256). As shown in Fig. 6, the image entropy of a well-exposed image is higher than that of an under/over-exposed image. Therefore, it is reasonable to use the entropy to find the optimal exposure ratio. The optimal exposure ratio \hat{k} is calculated by maximizing the image entropy of the enhancement brightness as

$$\hat{k} = \underset{k}{\operatorname{argmax}} \mathcal{H}(g(\mathbf{B}, k)). \quad (21)$$

Since the image entropy increases first and then decreases with the increase of the exposure ratio, \hat{k} can be solved by one-dimensional minimizer. To improve the calculation efficiency, we resize the input image to 50×50 when optimizing k .

V. EXPERIMENTS

To evaluate the performance of our method, we compare it with several state-of-the-art methods, including Multi Scale Retinex with Color Restoration (MSRCR) [45], Naturalness Preserved Enhancement algorithm (NPE) [16], dehazing based method (Dong) [38], Multi-deviation Fusion method (MF) [41], Illumination Estimation based method (LIME) [14] and Simultaneous Reflection and Illumination Estimation (SRIE) [46]. We test those methods on hundreds of low-light images from five public datasets: VV [47], LIME-data [14], NPE-data and its extension (NPE, NPE-ex1, NPE-ex2 and NPE-ex3) [16], DICM [3], and MEF [48]. The datasets are briefly introduced as follows:

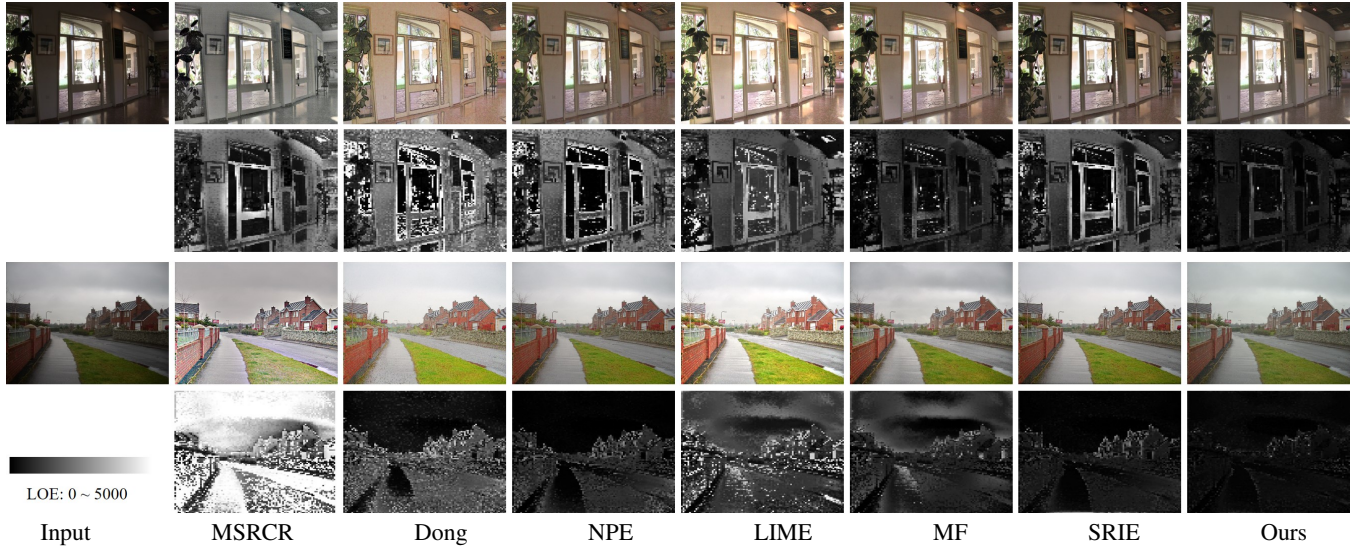


Fig. 7. Comparison of lightness distortion. The odd rows show the original image and the results of various enhancement methods, and the even rows show the visualization of each method's lightness distortion (RD).

TABLE I
QUANTITATIVE MEASUREMENT RESULTS OF LIGHTNESS DISTORTION (LOE).

	VV	LIME-data	NPE-data	NPE-ex1	NPE-ex2	NPE-ex3	DICM	MEF
MSRCR	2727.7	1835.5	1889.7	1870.3	1944.7	1776.3	1795.3	1686.2
Dong	853.35	1244	1012	1426.1	1096.3	1466.2	1180	1065.4
NPE	820.93	1471.3	646.34	840.83	775.82	1130	662.29	1158.2
LIME	1274.7	1323.8	1119.6	1321.9	1215.4	1319.1	1260.8	1079.4
MF	470.93	629.82	488.07	851.87	541.85	749.72	667.45	525.95
SRIE	551.39	823.61	533.24	653.05	564.49	760.76	623.32	754.2
Ours	287.22	478.57	308.12	319.93	323.72	378.65	351.82	325.86

VV¹. This dataset is collected by Vassilios Vonikakis in his daily life to provide the most challenging cases for enhancement. Each image in the dataset has a part that is correctly exposed and a part that is severely under/over-exposed. A good enhancement algorithm should enhance the under/over-exposed regions while not affect the correctly exposed one.

LIME-data². This dataset contains 10 low-light images used in [14].

NPE³. This dataset contains 85 low-light images downloaded from Internet. NPE-data contains 8 outdoor nature scene images which are used in [16]. NPE-ex1, NPE-ex2 and NPE-ex3 are three supplementary datasets including cloudy daytime, daybreak, nightfall and nighttime scenes.

DICM⁴. It contains 69 captured images from commercial digital cameras collected by [3].

MEF⁵. This dataset was provided by [48]. It contains 17 high-quality image sequences including natural sceneries, indoor and outdoor views and man-made architectures. Each image sequence has several multi-exposure images, we select one of poor-exposed images as input to perform evaluation.

In order to maintain the fairness of the comparison, all the codes are in Matlab and all the experiments are conducted on a PC running Windows 10 OS with 64G RAM and 3.4GHz CPU (GPU acceleration is not used). The parameters of our enhancement algorithm are fixed in all experiments: $\lambda = 1$, $\epsilon = 0.001$, $\mu = 1/2$, and the size of local window $\omega(x)$ is 5. The most time-consuming part of our algorithm is illumination map optimization. We employ the multi-resolution preconditioned conjugate gradient solver ($\mathcal{O}(N)$) to solve it efficiently.

A. Lightness Distortion

We use lightness order error (LOE) to objectively measure the lightness distortion of enhanced results. LOE is defined as

$$LOE = \frac{1}{m} \sum_{x=1}^m RD(x) \quad (22)$$

where $RD(x)$ is the relative order difference of the lightness between the original image P and its enhanced version P' for pixel x , which is defined as follows:

$$RD(x) = \sum_{y=1}^m U\left(\mathbf{L}(x), \mathbf{L}(y)\right) \oplus U\left(\mathbf{L}'(x), \mathbf{L}'(y)\right), \quad (23)$$

where m is the pixel number, \oplus stands for the exclusive-or operator, $\mathbf{L}(x)$ and $\mathbf{L}'(x)$ are the lightness component at location x of the input images and the enhanced images,

¹<https://sites.google.com/site/vonikakis/datasets>

²<http://cs.tju.edu.cn/orgs/vision/~xguo/LIME.htm>

³http://blog.sina.com.cn/s/blog_a0a06f190101cvon.html

⁴http://mcl.korea.ac.kr/projects/LDR/LDR_TEST_IMAGES_DICM.zip

⁵<https://ece.uwaterloo.ca/~k29ma/>

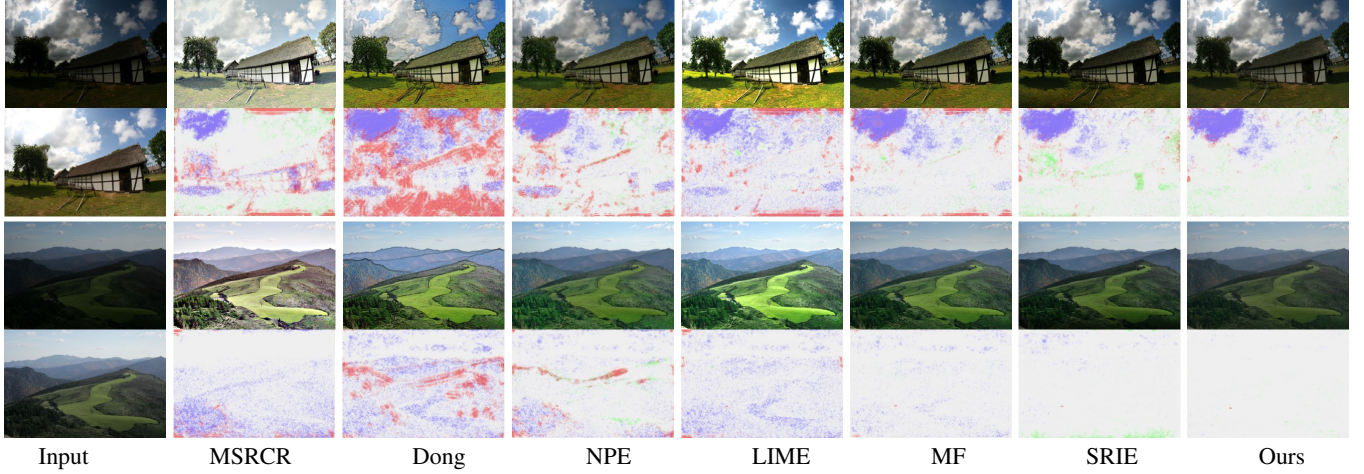


Fig. 8. Comparison of contrast distortion. The loss of visible contrast is marked in green, the amplification of invisible contrast is marked in blue, and the reversal of visible contrast is marked in red. Different shades of color represent different degrees of distortion.

TABLE II
QUANTITATIVE MEASUREMENT RESULTS OF VISUAL INFORMATION FIDELITY (VIF).

	VV	LIME-data	NPE-data	NPE-ex1	NPE-ex2	NPE-ex3	DICM	MEF
MSRCR	0.42134	0.24045	0.41425	0.29822	0.38625	0.65951	0.44966	0.27995
Dong	0.50477	0.32519	0.43440	0.38049	0.41687	0.50236	0.52637	0.35322
NPE	0.69006	0.50885	0.71471	0.58572	0.67769	0.74368	0.72497	0.52376
LIME	0.34932	0.20500	0.33934	0.28473	0.29498	0.38248	0.41498	0.22764
MF	0.72414	0.44752	0.63859	0.57687	0.61976	0.71747	0.70703	0.51293
SRIE	0.65968	0.52139	0.66528	0.58634	0.63547	0.69676	0.67866	0.55311
Ours	0.76098	0.74205	1.04930	0.70719	0.69787	0.76016	0.74524	0.60063

respectively. The function $U(p, q)$ returns 1 if $p \geq q$, 0 otherwise.

As suggested in [14], [16], down-sampling is used to reduce the complexity of computing LOE. We notice that LOE may change significantly when an image is down-sampled to different sizes since RD will increase as the pixel number m increases. Therefore, we down-sample all images to a fixed size. Specifically, we collect 100 rows and columns evenly to form a 100×100 down-sampled image.

As shown in Table I, our algorithm outperforms the others in all datasets. This means that our algorithm can maintain the naturalness of images well. We also provide a visualization of lightness distortion on two cases in Fig. 7, from which, we can find our results have the smallest lightness distortion. The results of MSRCR lose the global lightness order and suffer from severe lightness distortion. Although the results of LIME is visually pleasant, they are full of lightness distortion. The results of Dong, NPE, MF and SRIE can only retain the lightness order in the well-exposed regions.

B. Contrast Distortion

As aforementioned, the image that only differ in exposures can be used as a reference for evaluating the accuracy of enhanced results. DRIM (Dynamic Range Independent Metric) [49] can measure the distortion of image contrast without the interference of change in image brightness. We use it to visualize the contrast difference between the enhanced result and the reference image. As shown in Fig. 8, the

proposed method obtains the most realistic results with the least distortion.

C. Visual Information Distortion

To measure the distortion of visual information, we employ Visual Information Fidelity (VIF) [50] in reverse mode. As a full reference image quality assessment index, VIF models the quality assessment problem as a information fidelity criterion that quantifies the mutual information between the reference image C and the distorted image F relative to the information of C extracted by the HVS. VIF measure is given by

$$VIF = \frac{I(C; F)}{I(C; E)}, \quad (24)$$

where E is the image that the HVS perceives. The mutual information $I(C; F)$ and $I(C; E)$ represent the information that could be extracted by the brain in the reference and the test images respectively.

Like most of full reference image quality assessment methods, VIF were designed for and tested on degraded images. The normal version of VIF treats the original image as the reference image and the image outputted by algorithm as the degraded image. For image enhancement problem, however, the original image is the degraded one. Therefore, we employ VIF in reverse mode by specifying the enhanced version of the image as the reference and the original image as the degraded image. VIF provides consistently high value of correlation between subjective MOS (Mean Opinion Score) and its scores, as

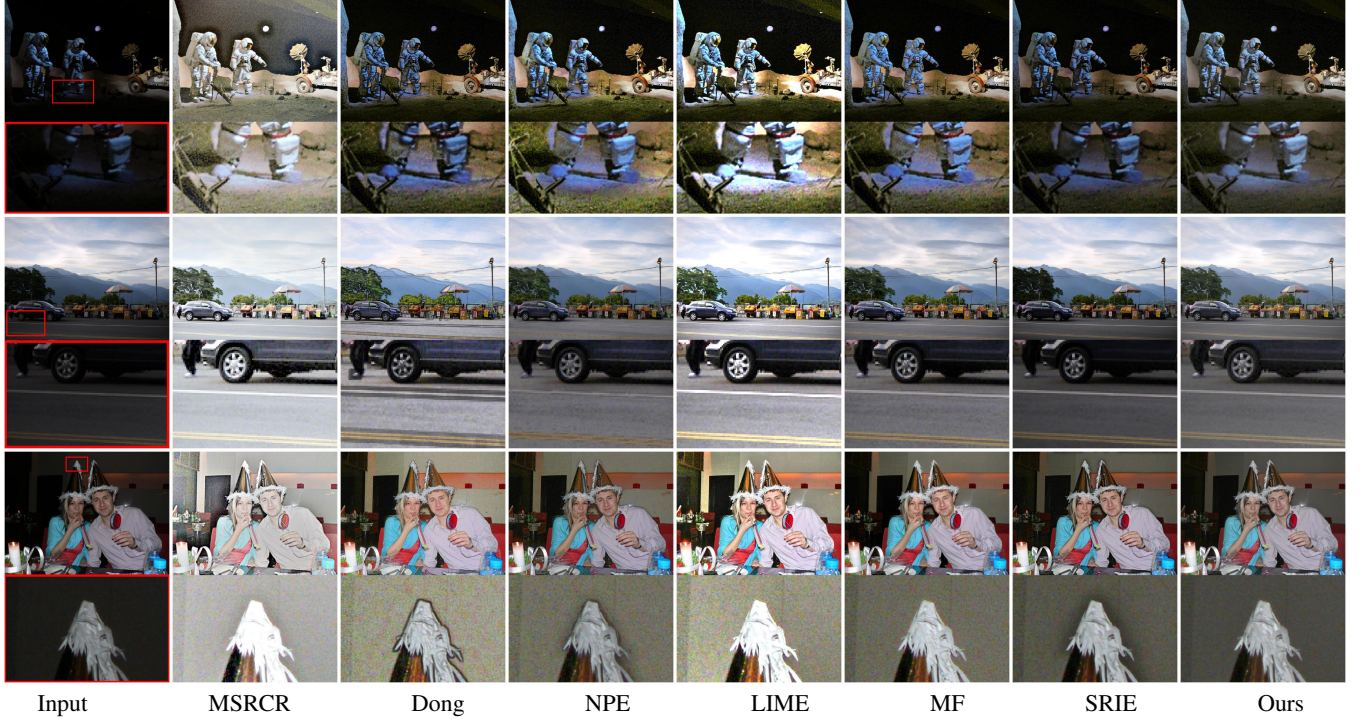


Fig. 9. Visual comparison among the competitors on different scenes.

shown in [51]. Besides, it is suitable for automating evaluation process of nonlinear image enhancement algorithms [52].

As shown in Table II, our algorithm outperforms the others in all datasets. This means that our algorithm can maintain the visual information of images well.

D. Time Cost

Fig. 10 gives the comparison among different methods in terms of time cost. Although SRIE and NPE produce small distortion, they are quite time-consuming. Our method achieves the smallest distortion than others with an acceptable time cost.

E. Subjective Evaluation

Fig. 9 shows more examples for visual comparison. Although the color correction post-processing in MSRCR can handle the color cast in some cases (*e.g.* underwater and hazy

images), it may make the results look whitish. Besides, in some dark show halo artifacts around sharp edges. The results of MSRCR shows severe halo artifacts around sharp edges and obvious noise in very dark areas (see the two astronauts) and suffer from detail loss in some bright areas (see the Christmas hat). The results of Dong is noisy and full of bold edges making it look like exaggerated art paintings. The results of LIME is so bright that many bright areas are saturated. Also, the noise in dark areas are amplified and de-noising method are therefore required to obtain better results. MF may introduce color over-enhancement (see the ground beneath the astronauts' feet) and SRIE may produce slight halo effects in some edges (see the Christmas hat).

VI. LIMITATION AND FUTURE WORK

Fig. 11 shows a failure case of our technique that the hair of the man turns to be grey because of over-enhancement. This is due to the dark area behind his head blending with his black hair. As shown in Fig. 11 (c), the hair is mistaken as the dark background in the estimated illumination map and therefore is enhanced along with the background. Such mistake is a result of the existing illumination map estimation techniques. This highlights a direction for future work. To avoid the over-enhancement due to the ignorance of the scene content, semantic understanding is required. With further refinement, we might employ the deep learning techniques to estimate the illumination map.

Besides, we only use two images to obtain the enhanced result. The over-exposure problem is remain unsolved. Images with smaller exposures than the input image should be considered in our framework to obtain a better result. We will address this problem as future work.

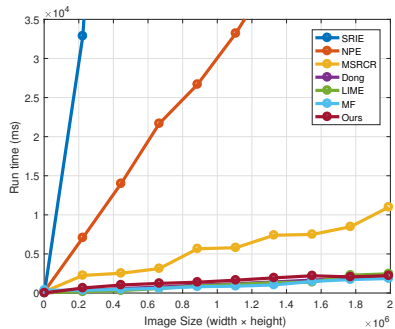


Fig. 10. Time comparison among different methods with varying image sizes



Fig. 11. An example of a failure case. (a) Raw image. (b) Enhanced result. (c) Estimated illumination \mathbf{T} .

VII. CONCLUSION

In this paper, we propose an exposure fusion framework and an enhancement algorithm to provide an accurate contrast enhancement. Based on our framework, we solve three problems: 1) We borrow the illumination estimation techniques to obtain the weight matrix for image fusion. 2) We introduce our camera response model to synthesize multi-exposure images. 3) We find the best exposure ratio so that the synthetic image is well-exposed in the regions where the original image under-exposed. The final enhanced result is obtained by fusing the input image and the synthetic image according to the weight matrix. The experimental results have revealed the advance of our method compared with several state-of-the-art alternatives. To encourage future works and allow more experimental verification and comparisons, we make the source code open on our project website⁶, as well as the relevant test code used to reproduce the experiment in the paper. We also provide the results of other competitors to facilitate the validation of quality measures.

APPENDIX DERIVATION OF CAMERA RESPONSE MODEL

The CRF model can be derived by solving the following comparametric equation (plug $g = \beta f^\gamma$ to $f(kE) = g(f(E), k)$):

$$f(kE) = \beta f(E)^\gamma. \quad (25)$$

Since β is positive, we can take the logarithm of both sides of Eq. 12:

$$\ln f(kE) = \ln \beta + \gamma \ln f(E). \quad (26)$$

Differentiate with respect to E , we get

$$k \frac{f'(kE)}{f(kE)} = \gamma \frac{f'(E)}{f(E)}. \quad (27)$$

The power function $\frac{f'(kE)}{f(kE)} = C_1 E^{a-1}$ where $a = \log_k \gamma$ can be a solution of Eq. 27. Then f can be solved by integration as

$$f(E) = \begin{cases} e^{C_1 \frac{E^a}{a} + C_2}, & \text{if } \gamma \neq 1, \\ C_3 E^{C_1}, & \text{if } \gamma = 1. \end{cases} \quad (28)$$

The constants C_1 , C_2 and C_3 can be determined by the restriction of $f(1) = 1$ and $f(k) = \beta$ (plug $f(1) = 1$ to Eq. 12) and the resulting f is obtained as follows:

$$f(E) = \begin{cases} e^{b(1-E^a)}, & \text{if } \gamma \neq 1, \\ E^c, & \text{if } \gamma = 1, \end{cases} \quad (29)$$

⁶<https://baidut.github.io/BIMEF>.

where a and b are model parameters in the case of $\gamma \neq 1$:

$$a = \log_k \gamma, \quad b = \frac{\ln \beta}{1 - \gamma}; \quad (30)$$

And c is model parameter in the case of $\gamma = 1$:

$$c = \log_k \beta. \quad (31)$$

REFERENCES

- [1] H. Xu, G. Zhai, X. Wu, and X. Yang, "Generalized equalization model for image enhancement," *IEEE Transactions on Multimedia*, vol. 16, no. 1, pp. 68–82, 2014.
- [2] T. Celik, "Spatial entropy-based global and local image contrast enhancement," *IEEE Transactions on Image Processing*, vol. 23, no. 12, pp. 5298–5308, 2014.
- [3] C. Lee, C. Lee, and C.-S. Kim, "Contrast enhancement based on layered difference representation," in *Image Processing (ICIP), 2012 19th IEEE International Conference on*. IEEE, 2012, pp. 965–968.
- [4] K. Arya, M. Pattanailk *et al.*, "Histogram statistics based variance controlled adaptive threshold in anisotropic diffusion for low contrast image enhancement," *Signal Processing*, vol. 93, no. 6, pp. 1684–1693, 2013.
- [5] C. Lee, C. Lee, Y.-Y. Lee, and C.-S. Kim, "Power-constrained contrast enhancement for emissive displays based on histogram equalization," *IEEE transactions on image processing*, vol. 21, no. 1, pp. 80–93, 2012.
- [6] T. Celik and T. Tjahjadi, "Contextual and variational contrast enhancement," *IEEE Transactions on Image Processing*, vol. 20, no. 12, pp. 3431–3441, 2011.
- [7] T. Arici, S. Dikbas, and Y. Altunbasak, "A histogram modification framework and its application for image contrast enhancement," *IEEE Transactions on image processing*, vol. 18, no. 9, pp. 1921–1935, 2009.
- [8] D. Coltuc, P. Bolon, and J.-M. Chassery, "Exact histogram specification," *IEEE Transactions on Image Processing*, vol. 15, no. 5, pp. 1143–1152, 2006.
- [9] S.-D. Chen and A. R. Ramli, "Contrast enhancement using recursive mean-separate histogram equalization for scalable brightness preservation," *IEEE Transactions on Consumer Electronics*, vol. 49, no. 4, pp. 1301–1309, 2003.
- [10] ———, "Minimum mean brightness error bi-histogram equalization in contrast enhancement," *IEEE transactions on Consumer Electronics*, vol. 49, no. 4, pp. 1310–1319, 2003.
- [11] S. M. Pizer, E. P. Amburn, J. D. Austin, R. Cromartie, A. Geselowitz, T. Greer, B. ter Haar Romeny, J. B. Zimmerman, and K. Zuiderveld, "Adaptive histogram equalization and its variations," *Computer vision, graphics, and image processing*, vol. 39, no. 3, pp. 355–368, 1987.
- [12] E. D. Pisano, S. Zong, B. M. Hemminger, M. DeLuca, R. E. Johnston, K. Muller, M. P. Braeuning, and S. M. Pizer, "Contrast limited adaptive histogram equalization image processing to improve the detection of simulated spiculations in dense mammograms," *Journal of Digital imaging*, vol. 11, no. 4, pp. 193–200, 1998.
- [13] Y.-T. Kim, "Contrast enhancement using brightness preserving bi-histogram equalization," *IEEE transactions on Consumer Electronics*, vol. 43, no. 1, pp. 1–8, 1997.
- [14] X. Guo, Y. Li, and H. Ling, "Lime: Low-light image enhancement via illumination map estimation," *IEEE Transactions on Image Processing*, vol. 26, no. 2, pp. 982–993, 2017.
- [15] L. Wang, L. Xiao, H. Liu, and Z. Wei, "Variational bayesian method for retinex," *IEEE Transactions on Image Processing*, vol. 23, no. 8, pp. 3381–3396, 2014.
- [16] S. Wang, J. Zheng, H.-M. Hu, and B. Li, "Naturalness preserved enhancement algorithm for non-uniform illumination images," *IEEE Transactions on Image Processing*, vol. 22, no. 9, pp. 3538–3548, 2013.
- [17] R. Kimmel, M. Elad, D. Shaked, R. Keshet, and I. Sobel, "A variational framework for retinex," *International Journal of computer vision*, vol. 52, no. 1, pp. 7–23, 2003.
- [18] D. J. Jobson, Z.-u. Rahman, and G. A. Woodell, "Properties and performance of a center/surround retinex," *IEEE transactions on image processing*, vol. 6, no. 3, pp. 451–462, 1997.
- [19] M. K. Ng and W. Wang, "A total variation model for retinex," *SIAM Journal on Imaging Sciences*, vol. 4, no. 1, pp. 345–365, 2011.
- [20] D. J. Jobson, Z.-u. Rahman, and G. A. Woodell, "A multiscale retinex for bridging the gap between color images and the human observation of scenes," *IEEE Transactions on Image processing*, vol. 6, no. 7, pp. 965–976, 1997.

- [21] K. Panetta, S. Agaian, Y. Zhou, and E. J. Wharton, "Parameterized logarithmic framework for image enhancement," *IEEE Transactions on Systems, Man, and Cybernetics, Part B (Cybernetics)*, vol. 41, no. 2, pp. 460–473, 2011.
- [22] K. A. Panetta, E. J. Wharton, and S. S. Agaian, "Human visual system-based image enhancement and logarithmic contrast measure," *IEEE Transactions on Systems, Man, and Cybernetics, Part B (Cybernetics)*, vol. 38, no. 1, pp. 174–188, 2008.
- [23] Y. Wang, S. Zhuo, D. Tao, J. Bu, and N. Li, "Automatic local exposure correction using bright channel prior for under-exposed images," *Signal Processing*, vol. 93, no. 11, pp. 3227–3238, 2013.
- [24] L. Yuan and J. Sun, "Automatic exposure correction of consumer photographs," *Computer Vision—ECCV 2012*, pp. 771–785, 2012.
- [25] G. Deng, "A generalized unsharp masking algorithm," *IEEE transactions on Image Processing*, vol. 20, no. 5, pp. 1249–1261, 2011.
- [26] Q. Shan, J. Jia, and M. S. Brown, "Globally optimized linear windowed tone mapping," *IEEE transactions on visualization and computer graphics*, vol. 16, no. 4, pp. 663–675, 2010.
- [27] J.-H. Hong, S.-B. Cho, and U.-K. Cho, "A novel evolutionary approach to image enhancement filter design: method and applications," *IEEE Transactions on Systems, Man, and Cybernetics, Part B (Cybernetics)*, vol. 39, no. 6, pp. 1446–1457, 2009.
- [28] S. T. McHugh, *Understanding Photography*. Cambridge in Colour, 2016.
- [29] H. Ibrahim and N. S. P. Kong, "Brightness preserving dynamic histogram equalization for image contrast enhancement," *IEEE Transactions on Consumer Electronics*, vol. 53, no. 4, pp. 1752–1758, 2007.
- [30] A. Beghdadi and A. Le Negrate, "Contrast enhancement technique based on local detection of edges," *Computer Vision, Graphics, and Image Processing*, vol. 46, no. 2, pp. 162–174, 1989.
- [31] E. Peli, "Contrast in complex images," *JOSA A*, vol. 7, no. 10, pp. 2032–2040, 1990.
- [32] R. Gonzalez and R. Woods, "Digital image processing: Pearson prentice hall," *Upper Saddle River, NJ*, 2008.
- [33] A. K. Jain, *Fundamentals of digital image processing*. Prentice-Hall, Inc., 1989.
- [34] C. Wang and Z. Ye, "Brightness preserving histogram equalization with maximum entropy: a variational perspective," *IEEE Transactions on Consumer Electronics*, vol. 51, no. 4, pp. 1326–1334, 2005.
- [35] A. M. Reza, "Realization of the contrast limited adaptive histogram equalization (clahe) for real-time image enhancement," *Journal of VLSI signal processing systems for signal, image and video technology*, vol. 38, no. 1, pp. 35–44, 2004.
- [36] J. A. Stark, "Adaptive image contrast enhancement using generalizations of histogram equalization," *IEEE Transactions on image processing*, vol. 9, no. 5, pp. 889–896, 2000.
- [37] M. Abdullah-Al-Wadud, M. H. Kabir, M. A. A. Dewan, and O. Chae, "A dynamic histogram equalization for image contrast enhancement," *IEEE Transactions on Consumer Electronics*, vol. 53, no. 2, 2007.
- [38] X. Dong, G. Wang, Y. Pang, W. Li, J. Wen, W. Meng, and Y. Lu, "Fast efficient algorithm for enhancement of low lighting video," in *2011 IEEE International Conference on Multimedia and Expo*. IEEE, 2011, pp. 1–6.
- [39] L. Li, R. Wang, W. Wang, and W. Gao, "A low-light image enhancement method for both denoising and contrast enlarging," in *Image Processing (ICIP), 2015 IEEE International Conference on*. IEEE, 2015, pp. 3730–3734.
- [40] X. Fu, D. Zeng, Y. Huang, X.-P. Zhang, and X. Ding, "A weighted variational model for simultaneous reflectance and illumination estimation," in *Proceedings of the IEEE Conference on Computer Vision and Pattern Recognition*, 2016, pp. 2782–2790.
- [41] X. Fu, D. Zeng, Y. Huang, Y. Liao, X. Ding, and J. Paisley, "A fusion-based enhancing method for weakly illuminated images," *Signal Processing*, vol. 129, pp. 82–96, 2016.
- [42] T. Mertens, J. Kautz, and F. Van Reeth, "Exposure fusion: A simple and practical alternative to high dynamic range photography," in *Computer Graphics Forum*, vol. 28, no. 1. Wiley Online Library, 2009, pp. 161–171.
- [43] J. Shen, Y. Zhao, S. Yan, X. Li *et al.*, "Exposure fusion using boosting laplacian pyramid," *IEEE transactions on cybernetics*, vol. 44, no. 9, pp. 1579–1590, 2014.
- [44] L. Xu, Q. Yan, Y. Xia, and J. Jia, "Structure extraction from texture via relative total variation," *ACM Transactions on Graphics (TOG)*, vol. 31, no. 6, p. 139, 2012.
- [45] A. B. Petro, C. Sbert, and J.-M. Morel, "Multiscale retinex," *Image Processing On Line*, pp. 71–88, 2014.
- [46] X. Fu, D. Zeng, Y. Huang, X.-P. Zhang, and X. Ding, "A weighted variational model for simultaneous reflectance and illumination estimation," in *Proceedings of the IEEE Conference on Computer Vision and Pattern Recognition*, 2016, pp. 2782–2790.
- [47] V. Voniakakis, R. Kouskouridas, and A. Gasteratos, "On the evaluation of illumination compensation algorithms," *Multimedia Tools and Applications*, pp. 1–21, 2017.
- [48] K. Ma, K. Zeng, and Z. Wang, "Perceptual quality assessment for multi-exposure image fusion," *IEEE Transactions on Image Processing*, vol. 24, no. 11, pp. 3345–3356, 2015.
- [49] T. O. Aydin, R. Mantiuk, K. Myszkowski, and H.-P. Seidel, "Dynamic range independent image quality assessment," *ACM Transactions on Graphics (TOG)*, vol. 27, no. 3, p. 69, 2008.
- [50] H. R. Sheikh and A. C. Bovik, "Image information and visual quality," *IEEE Transactions on image processing*, vol. 15, no. 2, pp. 430–444, 2006.
- [51] K. Gu, G. Zhai, W. Lin, and M. Liu, "The analysis of image contrast: From quality assessment to automatic enhancement," *IEEE transactions on cybernetics*, vol. 46, no. 1, pp. 284–297, 2016.
- [52] P. A. Kumar and P. Sankaran, "Visual information fidelity in evaluating retinex enhancement algorithms," in *Communications and Signal Processing (ICCP), 2014 International Conference on*. IEEE, 2014, pp. 167–171.